Soft Matter

PAPER

View Article Online
View Journal | View Issue

Cite this: *Soft Matter*, 2015, **11**, 7151

Magnetic field assisted programming of particle shapes and patterns†

Wenwen Xu, Yuyu Yao, John S. Klassen and Michael J. Serpe*

Received 22nd July 2015,
Accepted 3rd August 2015

DOI: 10.1039/c5sm01820j

www.rsc.org/softmatter

Anisotropic particles have generated an enormous amount of research interest due to their applications for drug delivery, electronic displays and as micromotors. However, up till now, there is no single protocol capable of generating particles of "patchy" composition with a variety of well-defined and predictable shapes. To address this, in this submission we dispersed magnetic nanoparticles (MNPs) in a non-magnetic fluid containing monomer and crosslinker. This solution was added to the surface of Teflon, which was submerged in the solvent 2,2,4-trimethylpentane. Under these conditions a round, stable droplet was formed on the Teflon. Upon exposure to a permanent magnet, the MNPs self-assembled into clusters with a variety shapes and sizes. The shape and size of the clusters depended on the magnetic field strength, which we controlled by systematically varying the distance between the magnet and the droplet. Interestingly, the shape of the liquid droplet was also influenced by the magnetic field. Upon polymerization, the MNP patterns and the droplet shape was preserved. We also show that very complex MNP patterns and particle shapes could be generated by controlling the distance between the drop and both a magnet above and below the droplet. In this case, the resulting patterns depended on whether the magnets were attracting or repelling each other, which was capable of changing the field lines that the MNPs align with. Overall, this approach is capable of generating particles with predictable MNP patterns and particle shapes without the use of any templates or complex synthetic steps. Furthermore, by using a sprayer (or similar approaches, *e.g.*, ink jet printing) this technique can be easily scaled up to produce many complex anisotropic particles in a short amount of time.

Introduction

The fabrication of particles with various and controllable shapes, and/or localized chemistry differences is of extreme interest for a variety of applications.[1,2] This has been driven by their ability to be used for drug delivery,[3] electronic paper,[4,5] micromotors,[6] and bar coding technology.[7] There are several methods proposed for anisotropic particle synthesis; the use of Pickering emulsions is one example.[8,9] Specifically, Granick and coworkers,[10,11] adsorbed particles at the interface of wax and water, one half of the particle was shielded from the water (due to its attachment to the wax) while the other half remained exposed to the water, which allows for its easy chemical modification independent of the other half. One downfall of this approach is the fact that particles can be detached from the wax during the functionalization, leading to homogenous particle modification, lowering the yield of the asymmetrically modified (Janus) particles. Another approach that is widely used for generating Janus particles is to use microfluidic devices.[5,12] However, this method is not universal, and can be cumbersome to optimize to yield the desired particles. For example, flow rate,[13] microchannel chemistry,[14,15] and microchannel shape[16] have to be carefully tuned and optimized to make specific particles. Yet another way to make Janus particles is *via* block copolymer self-assembly.[17] However, solvent selection for phase separation, the requirement for precisely defined molecular composition, and very carefully controlled environments (temperature, humidity, *etc.*) makes this method tedious to implement.[18] While generating basic Janus particles can be cumbersome, the complexity is increased if patches of controlled and defined sizes are required (Janus balance). Controlling these parameters is very important for directing the assembly and attachment of anisotropic particles.[19,20]

The generation of non-spherical Janus particles is another very interesting area because it can yield self-assembled structures with much more complex architectures not available with spheres.[21] This is especially challenging due to the fact that most cases obtained spherical Janus particles which offer the lowest surface-to-volume ratio and minimizes the interfacial energy. While this is the case, such particles have been realized. For example, Müller's group synthesized triblock copolymer to

Department of Chemistry, University of Alberta, Edmonton, Alberta, T6G 2G2, Canada. E-mail: michael.serpe@ualberta.ca

† Electronic supplementary information (ESI) available. See DOI: 10.1039/c5sm01820j

yield disc/sheet like Janus particles.[22] By asymmetric wet-etching at the Pickering emulsion interface, Yang's group also fabricated non-spherical silica Janus particles.[23] However, generally speaking, those methods above are complicated. Therefore, simpler and more efficient methods are highly desirable to generate non-spherical Janus particles.

To address the above needs, in this paper, we developed a new method for anisotropic particle fabrication, which is simple, effective and versatile. This approach utilizes interfacial polymerization of a monomer/crosslinker solution that has magnetic nanoparticles (MNPs) dissolved. By using magnetic fields, and modulation of their strength and the magnetic field line directions, we were able to generate very complex anisotropic particles with well-defined shapes and conformations. These particles not only offer a diverse range of flexibility when it comes to structural and compositional diversity, but they can find utility as building blocks for microactuators in the pharmaceutical industry for cellular manipulation.[24,25] We point out that this approach can be used to synthesize complex particles much smaller than what is presented here by simply depositing smaller volumes of liquid on the teflon. Furthermore, the same techniques that can be used to make smaller particles can also be used to make multiple particles in very short amounts of time; *e.g.*, nebulization or ink jet printing.

Experimental

Materials

2-Hydroxylethylmethacrylate (HEMA) (≥97%), poly(ethylene glycol) diacrylate (PEGDA) (M_n = 700), 2,2,4-trimethylpentane (TMP) (≥99%), ammonium persulfate (APS) (≥98%), *N*,*N*,*N*′,*N*′-tetramethylethylenediamine (TEMED) (≥99%) as well as Fe(II, III) oxide nanoparticles (50 nm–100 nm diameter) with no surface modification was purchased from Sigma Aldrich (Oakville, Ontario). Ultra high-pull Neodymium-Iron-Boron (NdFeB) magnets (5 × 5 × 1 cm) were purchased from McMaster-Carr Company (Elmhurst, IL). Deionized water (DI water) with a resistivity of 18.2 MΩ cm was used and obtained from a Milli-Q Plus system (Millipore Co., Billerica, MA). Polyetrafluoroethylene (PTFE) was provided by Johnston Industrial Plastics (Edmonton, Alberta).

Preparation of anisotropic particles

Fe(II, III) oxide magnetite MNPs (0.37 M), 2-hydroxylethylmethacrylate (HEMA) (3.52 M), and poly(ethylene glycol) diacrylate (PEGDA) (0.23 M) aqueous solution was used as the "pre-gel" solution. Aqueous solutions of the initiator ammonium persulfate (APS) (0.44 M) and accelerator *N*,*N*,*N*′,*N*′-tetramethylethylenediamine (TEMED) (0.67 M) were also used. 10 μL of the APS solution and 10 μL of the TEMED solution were added to 0.1 mL of the pre-gel solution and mixed, and 5 μL aliquots (in most cases) manually added to the PTFE–TMP interface. The external magnetic field was applied by custom-build magnetic stage where two NdFeB magnets were fixed above and below the Petri dish, with positioning screws to accurately and precisely control the distance between the Petri dish and the magnets. The polymerization was allowed to proceed for 1 h before the particles were collected. The mechanism of free-radical polymerization accelerated by TEMED has been studied in detail previously.[26] Briefly, TEMED reacts with APS through redox reaction, which produces free radicals, which can initiate polymerization. Thermal gravimetric analysis (TGA) was performed on the resultant particles to determine how much of the particle mass could be attributed to MNPs, and the data are shown in ESI.† From the data, we can determine that the MNPs account for ∼6% (w/w) of the particle mass.

Instrumentation

Photographs of the particles were obtained using a Nikon camera equipped with a 105 mm Nikon macrolens (Nikon, Ontario, Canada). Optical microscopy (Olympus IX-70 Melville, New York, USA)) was used to image smaller particle. Contact angle was measured using an automated goniometer with drop image Advanced V2.4 software from rame-hart Instrument Co. (New Jersey, USA). Magnetic measurements of the purchased MNPs were performed using a Quantum Design 9T-PPMS magnetometer with fields up to 1 T at room temperature. TGA was performed using a Perkin Elmer Pyris TGA1 under a nitrogen atmosphere, heating from 25.00 °C to 600.00 °C at scan rate 10.00 °C min^{-1}.

Results and discussion

Patterned particles were synthesized by suspending Fe(II, III) oxide magnetic nanoparticles (MNPs) (0.37 M) in 2-hydroxylethylmethacrylate (HEMA) (3.52 M), and poly(ethylene glycol) diacrylate (PEGDA) (0.23 M), which was referred to as the "pre-gel" solution (non-magnetic liquid carrier). Aqueous solutions of ammonium persulfate (APS) (0.44 M) as initiator and *N*,*N*,*N*′,*N*′-tetramethylethylenediamine (TEMED) (0.67 M) as accelerator were made, and were mixed with the pre-gel solution to make particles. In one case, 100 μL of the pre-gel solution was mixed with 10 μL of the APS solution and 10 μL of the TEMED solution. After this solution was shaken for ∼5 s, 5 μL droplets were dispensed *via* digital pipet onto a piece of Teflon that was submerged in 2,2,4-trimethylpentane (TMP) all in a Petri dish. Under these conditions, the drops formed nearly perfect spheres on the Teflon surface. This was expected from previously published results.[27] In this case, in the absence of a magnetic field, the MNPs were randomly distributed in the droplet (and polymerized particle) due to Brownian motion; the resultant particle shape was spherical. However, when an external magnetic field is applied, chain-like structures (clusters) are observed within 1 s, which are locked into place *via* polymerization (Fig. 1d). MNP assembly on this time scale has been observed previously, and thus was expected.[28] Cluster formation has also been observed in magnetorheological fluids, which were extensively studied.[29] Although, magnetorheological fluids are typically composed of magnetic particles with micron-size dimensions, while our particles have nano-dimensions. Thus, while the

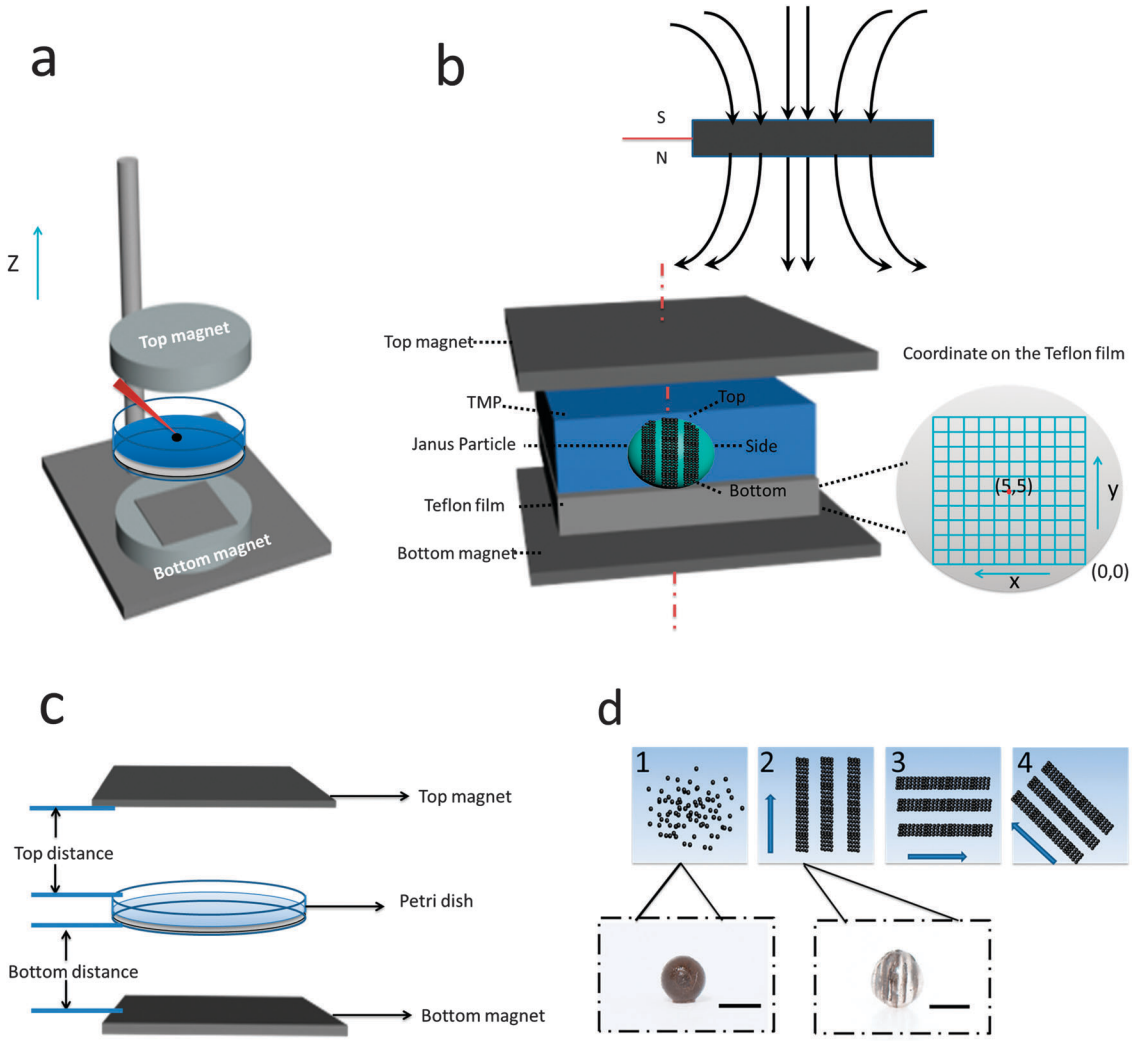

Fig. 1 (a) Schematic of the setup used for the anisotropic particle synthesis. The polymerization solution was manually dispensed onto the Teflon, which was submerged in TMP. The distance between the magnets and the Petri dish could be very carefully controlled using positioning screws attached to the magnets. (b) Side view of the setup, with "top", "side", and "bottom" defined. Furthermore, the coordinates on the Teflon are defined – each square is 5 mm^2. (c) The relative distance between the magnets and the Petri dish (d) schematic illustrating how (1) the MNPs are randomly dispersed at zero field, with corresponding photograph of the resulting particle. (2, 3 and 4) Schematic of the MNP chain configuration in the presence of a magnetic field of different directions, with a corresponding photograph of a representative particle. All scale bars in the pictures are 1 mm.

behavior here should be similar to magnetorheological fluids, it is not necessarily the case.

Fig. 1(a) shows a schematic of the setup we used to fabricate anisotropic particles with complex structures and shapes. The setup is composed of a stand capable of holding the Petri dish assembly used above, but also allows for control of the distance between the two magnets and the Petri dish. We point out that the holders for two magnets were made of aluminum, which made it extremely strong and stable. Fig. 1(b) shows the simplified side view of our system. It is important to note that the magnetic field is not uniform over the whole magnet area, so for these experiment, it was important to record the position of every drop relative to the magnet. In order to do this, a coordinate system was used as defined in Fig. 1(b). For our experiments, we always made sure to fix the position of the magnets and the coordinate system, such that it was the same from experiment to experiment. For these studies, it was important to consistently define and measure the proximity of the magnets to the particles. This is detailed in Fig. 1(c), which shows the top distance as the distance between the bottom of the top magnet and the top edge of the Petri dish, while the bottom distance is the distance between top of the bottom magnet and the bottom face of the Petri dish. The same Petri dish and Teflon was used for all experiments – the wall thickness of the Petri dish was 2 mm with a depth of 1 cm and diameter is 8.5 cm; the Teflon was 3 mm thick and had a diameter is 8.2 cm. This way of measuring distance was chosen due to its ease and reproducibility; it was also beneficial because it didn't disturb the system. For demonstration purposes, Fig. 1(d) shows how an external magnetic field could be used to manipulate magnetic particles in the droplet. If polymerization of the drops composed of MNPs proceeded in the presence of a magnetic field, by properly

positioning the magnet near the Petri dish used for polymerization, the MNPs could align themselves with the magnetic field lines. Furthermore, when there is applied magnetic field, MNPs obtain an induced dipole moment which causes them to self-assemble into chain structures parallel to the external field lines to minimize the free energy of the system.[30] To explain how the magnetic field can be used to assemble the MNPs in the pre-gel solution prior to polymerization, the ratio of the magnetic energy to thermal energy as is shown in eqn (1) needs to be considered, which can be expressed as[30,31]

$$\lambda = \frac{W_m}{K_B T} = \frac{\mu_0 \vec{m}^2}{16\pi r^3 K_B T} \quad (1)$$

$$\vec{m} = \frac{4}{3}\pi r^3 \chi_{eff} \vec{H} \quad (2)$$

$$\chi_{eff} = 3\frac{\mu_p - \mu_s}{\mu_p + 2\mu_s} \quad (3)$$

$$\chi_p = \mu_p - 1 \quad (4)$$

where W_m: magnetic inter-particle interaction energy; μ_0: magnetic permeability of vacuum; K_B: Boltzmann constant; T: temperature in Kelvin; r: the radius of the particle; $\vec{m}$: induced magnetic moment; $\vec{H}$: external field strength; χ_{eff}: effective susceptibility; μ_p: relative permeability of MNPs; μ_s: relative permeability of solvent and it is equal to the vacuum permeability which is a universal constant; χ_p is the MNPs' susceptibility. In our case, χ_p for MNPs is 0.38, their diameter is about 50 nm and the maximum field strength for the permanent magnet is 1777 G. Fig. S1(a) in ESI† shows that saturation magnetisation is achieved only when the external field is above 5000 G, which demonstrates that eqn (1) is suitable for our system. Specifically, λ is the ratio of magnetic energy of MNPs compared to MNPs' thermal energy (Brownian motion). Therefore, when λ is high, the magnetic energy dominates thermal energy and the chain structure forms. According to the above equations, using the above parameters, λ in our system is $\sim$31, indicating that magnetic forces play a dominant role over thermal fluctuation which can make the particles self- assemble into stable chain clusters. Therefore, the role of the external field is to align MNP chains with the external field, assisting stacking of chains along the axis of the field and then draw them towards the ends of the permanent magnets where the magnetic field gradient is the steepest. The magnet movement and relative positions, and the dipole forces between MNPs can allow the formation of different patterns and even change the shape of the droplet, which we will talk about in detail later.

We first investigated the case of a single magnet located below the Petri dish and droplet. The influence of the magnetic field on the droplet shape is shown in Fig. 2(a). As can be seen, well-known magnetowetting phenomena are observed.[32] That is, the applied field forces the droplet to flatten (relative to no applied magnetic field) and the contact angle decreases. Furthermore, the magnetic field can cause the MNPs to form patterns, which are easily visible after the particles polymerize,

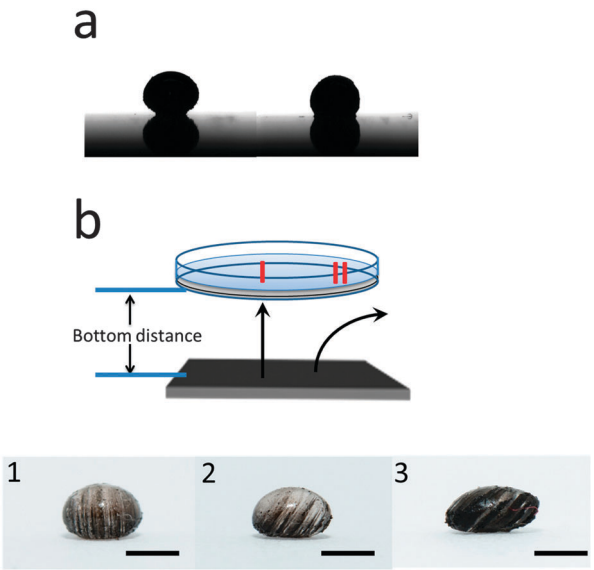

Fig. 2 (a) Photograph of a pregel droplet deposited at the (5, 5) position, with a magnet below the droplet. (left) When the magnet is 4 cm away the contact angle is 165.45 ± 0.07, while it is 146 ± 1 when the magnet is 0.3 cm away. (b) Photographs of the resulting particles polymerized with the magnet below the droplet all synthesized at a distance of 0.3 cm, for 1 at position (5, 5) which is the center of the Teflon film (place I), for 2 at position (1, 2) which is at the edge of the Teflon film (place II), 3 is also synthesized at position (1, 2) with the concentration of MNPs increased to 0.55 M. All scale bars in the pictures are 1 mm.

which locks in the MNP structure in the particle. This behavior is clearly shown in the photographs in Fig. 2(b), which shows MNP chains being formed. The alignment of the MNPs in the magnetic field appear similar to what was observed by the Pyun group.[33]

The reason for the parallel MNP chain structure formation is due to the angular dependence of the dipolar interaction. The external field can cause particles to generate a preferred head-to-tail alignment. Closer examination revealed that the uniform dipole orientation causes a second possibility: side-by-side particles with aligned dipoles resulting in dipole repulsion. This angular dependence of the dipolar interaction effectively eliminates half of the possible particle binding events by making it impossible for particles to bind with each other when they approach from a direction that is orthogonal to the applied field. Regardless of the field direction, the patterns on the particles we obtained are always chains parallel to each other as in Fig. 2(b). The direction of the magnetic field also has an influence on the pattern of the particle. When the MNP-containing droplet is added to a different coordinates on the Teflon (*i.e.*, different parts of the magnet), it is exposed to a different magnetic field and magnetic field line directions.

In all the upcoming examples, we show the relative position between the Petri dish and magnets and the magnetic field line is indicated as a black arrow. As can be seen in Fig. 2(b-1), when the droplet was placed at the position (5, 5), which is the center of the magnet, the vertical field lines will force the MNPs to self-assemble into vertical chains. We point out that "vertical" is

parallel to the "z-axis" in Fig. 1(a), while horizontal is perpendicular to the "z-axis". On the other hand, when the droplet was placed at position (1, 2) where the field line is "diagonal", there will be diagonal chains formed and obvious deformation of the droplet shape, see Fig. 2(b-2). Photographs were taken of each resulting particle, one showing a side view of the particle as it was positioned on the Teflon, the other two are of the top (near the top magnet) and bottom (near the bottom magnet) of the particle. The top and bottom views for all the particles synthesized here are shown in the ESI.†

Under an external magnetic field, the droplets are subject to two opposing forces: the TMP/water (pre gel solution) droplet interfacial tension and interaction between the induced magnetic field on the MNPs.[34,35] The former tends to minimize the interface between the TMP/water, while the latter favors an extended interface to minimize the dipole–dipole interactions. In our system, the dipole–dipole interaction is so strong that MNPs form the chainlike structures and the droplet shape is deformed in order to increase the interfacial area to attenuate the dipole interactions. Therefore, when we increased the concentration of MNPs, we also observed much more pronounced particle shape distortion, *e.g.*, see Fig. 2(b-3).

Fig. 3 shows particles synthesized when a single magnet is located above the Petri dish instead of below. When the distance between top magnet and Petri-dish is 5 cm, MNPs tend to migrate to the top side which has the strongest field strength and as a result, a teardrop shape particle is formed, Fig. 3(1). When the magnetic field is strong enough, rods can be formed that protrude out of the main droplet. After polymerization, the structure is locked in; see Fig. 3(2). The key characteristics of the ferromagnetic MNPs used in our experiment, that distinguishes them from their paramagnetic counterparts, is the quasi-irreversibility of the MNP chain formation process. When the external magnetic field is partially removed, the MNPs partially demagnetize very quickly, and gravity plays an important role in this case and draws the MNPs rod back into the droplet. However, MNPs still have magnetic attraction, which hold them together and dominate over Brownian motion, which would force the MNPs to redisperse. Therefore, as can be seen in Fig. 3(3 and 4), we can change the length of the rod that is formed on the particles.

We also synthesized particles in the presence of two of the same permanent magnets, one above and below the Petri dish. These magnets can either be attracting or repelling one another. This is shown in Fig. 1. Depending on the configuration, we can generate different particle shapes and MNP patterns formed. In this case, we make the assumption that the magnet material's coercivity is sufficiently high that the magnetic field from the first magnet cannot substantially alter the magnetization of the second magnet.

Fig. 4 shows that when the two magnets generate attractive forces, vertical MNP chains will again be generated. As is shown, they are parallel to the external field line. Although, in this case, the MNP chain formation can be controlled. For example, when the distance between the bottom magnet and

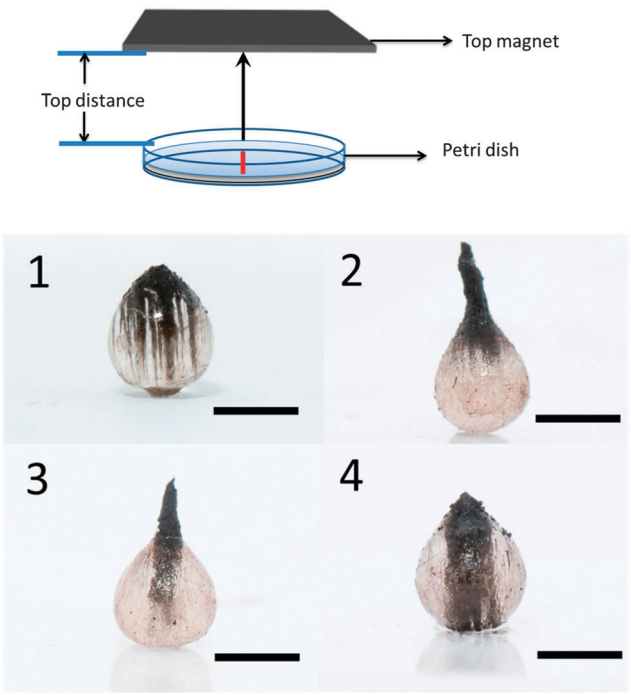

Fig. 3 Photographs of the resulting particles polymerized with the magnet above the droplet at a distance of (1) 5 cm, and (2) 4.5 cm. For (3), first the magnet was <4.5 cm to make the rod structure as shown in 2, then moved to a distance of 5 cm. As can be seen, the gravitational force pulls the rod back into the particle. 4 is the same as 3, but the final distance of the magnet is 6 cm, which allows even more of the rod to enter the particle to make a stripe. All particles were synthesized at the (5, 5) position, which is the center position (I). All scale bars in the pictures are 1 mm.

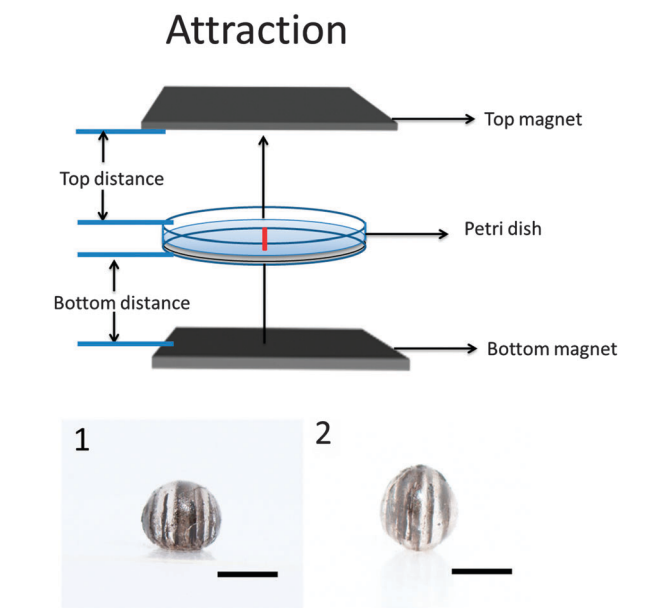

Fig. 4 Photographs of the resulting particles polymerized with a magnet above and below the droplet in the attractive regime. The bottom distance is fixed as 2 cm and both particles are synthesized at center (place I) (5, 5). Top distance for (1) is 5 cm and for (2) is 3.5 cm. All scale bars in the pictures are 1 mm.

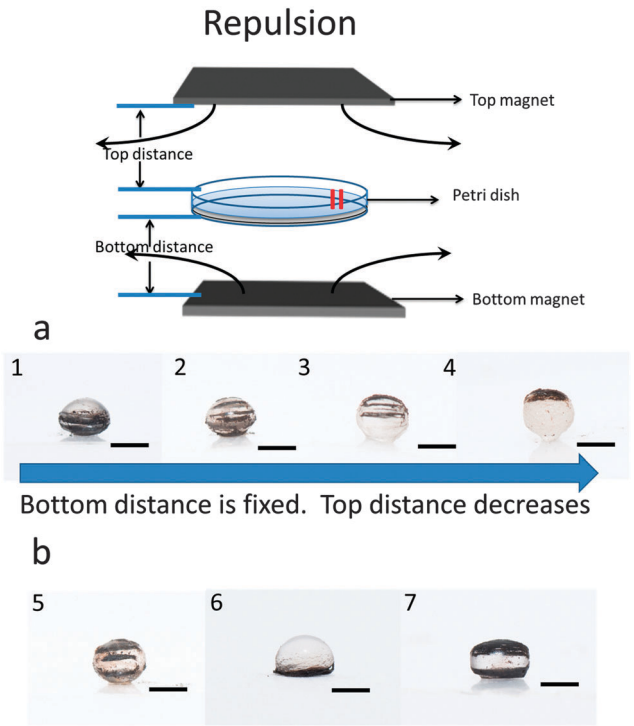

Fig. 5 Photographs of the resulting particles polymerized with a magnet above and below the droplet in the repulsive regime. All the particles are synthezed at the edge area (place II) of the Teflon film due to the influence of the external magnetic field. For (a), the bottom magnet distance is fixed at 2 cm and they are all synthezised at place (1, 1); the top distance gradually decreased: for (1) is 5 cm, for (2) is 4 cm, for (3) is 3.5 cm, for (4) is 3 cm. As the top magnet distance decreases, it gradually changes the coverage of the horizontal stripes on the particle. In part (b), we can control the number of the stripes on the particle (compare (5) with (2)). (5) was synthesized at position (1, 1) on the Teflon, the top distance is 3 cm, the bottom distance is 1 cm. For (6) and (7), they were both synthesized at position (2, 3) on the Teflon and bottom distance is 0.3 cm. The top distance for (6) is 5 cm, for (7) is 2.4 cm. All scale bars in the pictures are 1 mm.

Petri dish is fixed at 2 cm, decreasing the distance between the top magnet and Petri dish will increase the magnetic field flux density. As a result, the number of formed chains will decrease and the chains will become thicker.

When the two magnets are generating repulsive forces, the results shown in Fig. 5 are obtained; this is completely different than the attractive case. For example, at certain distances, opposing fields cancel each other out, leading to localized magnetic field minima. As a result, particles will experience forces that go outwards to the surrounding region of higher magnetic field.[24,36] By controlling the local magnetic field strength, we can control the number and coverage of MNP chains on the particles. The coverage of horizontal chains can be controlled through adjustment of the relative distance between the top magnet and the Petri dish. In Fig. 5(a), we fix the distance between the bottom magnet and Petri dish at 2 cm, and the distance between the top magnet and the Petri dish is varied. When the top magnet is 5 cm from the Petri dish, the bottom magnetic field is stronger than the top one, and the chains mainly formed at the bottom of the particle (Fig. 5(1). When the distance between the top magnet and the Petri dish is decreased to 4 cm, the chains are observed throughout the particle, Fig. 5(2). When the distance between the top magnet and the Petri dish is decreased to 3.5 cm, the chains mainly occupy at the top half of the particle, Fig. 5(3). Finally, when the distance between the top magnet and the Petri dish is decreased to 3 cm, the MNP chains are mainly at the top side of the particle Fig. 5(4). When the repulsive magnetic field direction is horizontal (at certain magnet–magnet distances), the shape of the particle becomes ellipsoidal, as seen in Fig. 5(1–3). When the top magnet is close enough to the Petri dish (<3 cm), the drop will pull off the Teflon and float on the TMP/air interface to generate a particle with a flat surface (see ESI†). Additionally, by comparing Fig. 5(5) with Fig. 5(2), it can be seen that the number of MNP chains in the particles can be controlled by controlling the magnet–magnet distance. When the distance between the bottom magnet and Petri dish is 0.3 cm, and the top magnet is "far away" from the Petri dish (5 cm), we observed a hemispherical particle with off the MNP chains on the bottom Fig. 5(6). However, when both magnets are very close to the Petri dish (bottom is 0.3 cm and top is 2.4 cm), the particle became a semi-cuboid (Fig. 5(7)).

Next, we showed that the anisotropic particles generated from these experiments could be differentially manipulated depending on the MNP patterns in the particles and the magnetic field. As is shown in Fig. 6, the MNP chains in the particles are oriented parallel to the magnet's field line. In Video ESI,† we show that the same particle in Fig. 6 can be precisely controlled by an external magnet. Specifically, the anisotropic particle rotates and moves in a fashion that is synchronized with the external field, using a single rotation

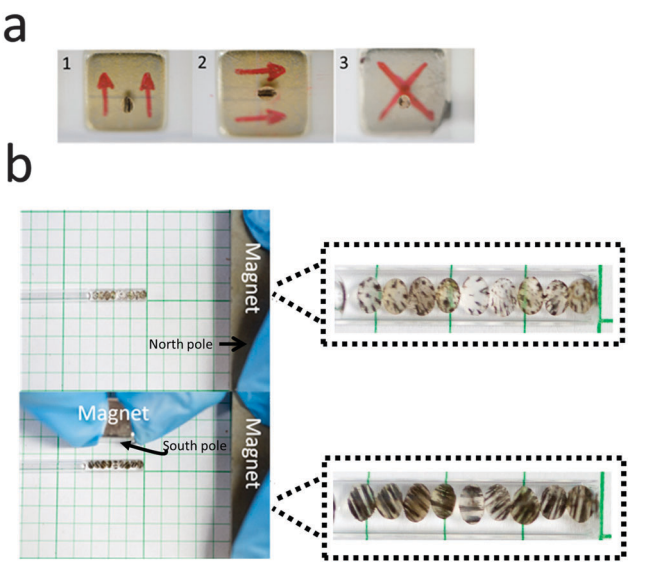

Fig. 6 (a) A representative patterned particle is aligned with the magnet's field lines and moves in response to its changes – the field lines are indicated by the red marks on the magnet. (b) Representative anisotropic particles can orient themselves according to the field line orientations, which can be influenced by changing the distance between the magnets and the particles.

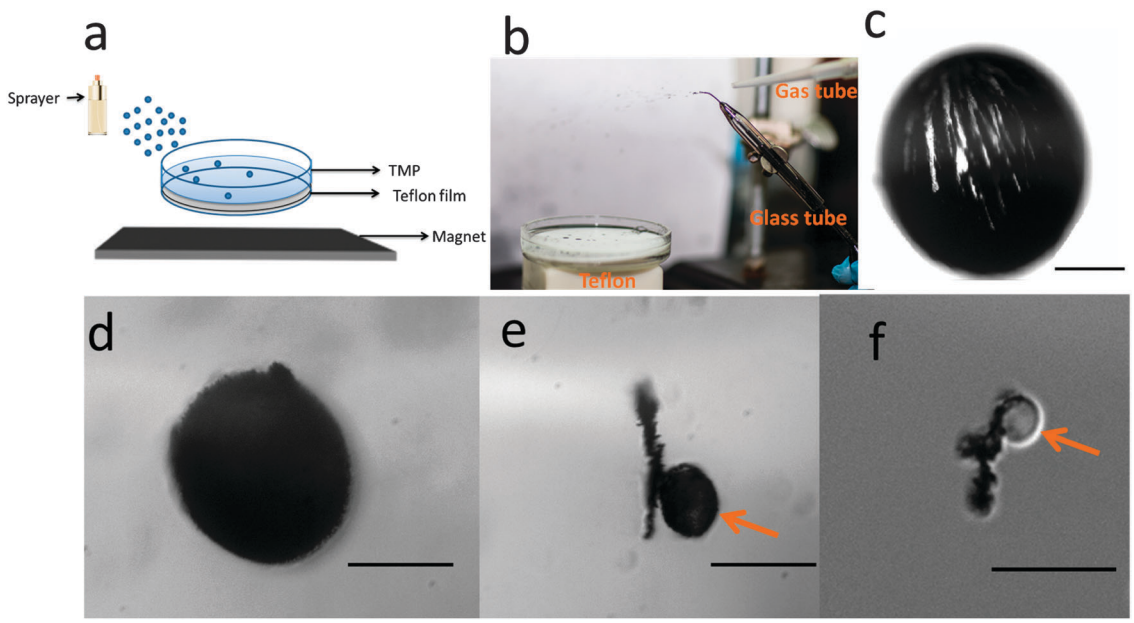

Fig. 7 (a) Schematic illustration of the system used to prepare anisotropic particles *via* a spray bottle; (b) a tube used to supply nitrogen gas is directed onto a glass tube, out of which monomer/photoinitiator is being pumped; the gas dispersed the solution into a fine mist, which settled on the Teflon film, which underwent photopolymerization to generate particles; (c) microscope image of a representative anisotropic particle with a diameter of ~400 μm – the scale bar is 100 μm. (d–f) Microscope images of various particles that can be produced using the procedure in (b), (d and e) the scale bar is 50 μm; (f) the scale bar is 20 μm.

axis. It is also very easy to control the translational movement of the anisotropic particle under external magnetic field. Finally, we showed that our particles are very sensitive to external fields, and are capable of assembling into unique anisotropic patterns shown in Fig. 6. To accomplish this, synthesized anisotropic particles were added to a capillary tube with a diameter of ~2 mm and filled with DI water. External magnets were placed near the tube, which resulted in particle orientation, which could be easily switched by changing the relative distances between the magnets and the tube.

Finally, we showed that the synthesis of anisotropic particles could be scaled up, such that many particles could be synthesized in a simple manner and in a short time. In one example, we added the monomer solution to a spray bottle, and simply sprayed the monomer solution into the Petri dish assembly; the generated aerosol particles form the droplets that polymerize on the Teflon. This is illustrated in Fig. 7(a), and particles synthesized in this way can be seen in Fig. S6(a and b) (ESI†). An even more efficient approach to synthesize many particles simply and quickly, while allowing for the particle size to be easily tuned, is shown in Fig. 7(b). This approach simply uses a high pressure nitrogen gas stream directed at the tip of a tube, out of which a monomer solution could be pumped. The gas stream is capable of generating a fine mist, and the mist droplets (containing in this example monomer and photoinitiator) settle onto the Teflon surface. The drops on the Teflon could be polymerized by simple exposure to UV light. For this experiment, we used a pre-gel solution composed of poly(ethylene glycol) diacrylate (PEGDA (95% v/v)), photointiator 2,2-dimethoxy-2-phenylacetophenone (5% v/v) and MNPs (amount could be varied). The gas stream pressure and angle relative to the tip of the monomer solution delivery tube can be easily tuned to adjust the particle size. Microscope images (obtained with an Olympus optical microscope) of representative particles that were generated in this manner are shown in Fig. 7(c–f) as well as in ESI.† As can be seen from the representative microscope images, particles with diameters in the range of 5–400 μm could be readily generated. Furthermore, Fig. 7(c) shows that the structure of the magnetic particles could be retained after polymerization.

Conclusion

Using a simple setup composed of magnets interacting with MNPs, very complex particle structures, with very intricate MNP patterns locked inside each particle could be synthesized. The exact particle shape and arrangement of the MNP chains in the particles depended on if one or two magnets were used, and their distance away from the synthesis vessel. We showed that the synthetic conditions and setup are extremely robust, and can be used to synthesize many particles with predefined shape/configuration in a very reliable and reproducible manner. We also showed that the particles could be manipulated by external magnetic fields. Finally, the synthetic approach was shown to be scalable, such that many particles could be synthesized in parallel and the diameter can be reduced to hundreds of microns with system modification. These systems have many interesting potential applications for patterning, actuation, and for memory storage and encryption applications, which will be the topic of future studies.

Acknowledgements

MJS acknowledges funding from the University of Alberta (the Department of Chemistry and the Faculty of Science), the Natural Sciences and Engineering Research Council of Canada (NSERC), the Canada Foundation for Innovation (CFI), and the Alberta Advanced Education & Technology Small Equipment Grants Program (AET/SEGP). WX acknowledges Alberta Innovates – Technology Futures for a Graduate Student Scholarship. We thank Prof. Mark Freeman for helpful discussions, Prof. Arthur Mar for assistance with the magnetic property measurements, and Prof. Ratmir Derda for helping with particle synthesis with a microfluidic device. We also thank Vincent Bizon for the constructing the magnet positioning/synthesis apparatus used in this study.

References

1 S. C. Glotzer, *Science*, 2004, **306**, 419.
2 A. Walther and A. H. Müller, *Chem. Rev.*, 2013, **113**, 5194.
3 S. Mitragotri and J. Lahann, *Nat. Mater.*, 2009, **8**, 15.
4 T. Nisisako, T. Torii, T. Takahashi and Y. Takizawa, *Adv. Mater.*, 2006, **18**, 1152.
5 S. H. Kim, S. J. Jeon, W. C. Jeong, H. S. Park and S. M. Yang, *Adv. Mater.*, 2008, **20**, 4129.
6 W. Gao and J. Wang, *ACS Nano*, 2014, **8**, 3170.
7 H. Lee, J. Kim, H. Kim, J. Kim and S. Kwon, *Nat. Mater.*, 2010, **9**, 745.
8 D. Suzuki, S. Tsuji and H. Kawaguchi, *J. Am. Chem. Soc.*, 2007, **129**, 8088.
9 B. Liu, W. Wei, X. Qu and Z. Yang, *Angew. Chem., Int. Ed.*, 2008, **120**, 4037.
10 L. Hong, S. Jiang and S. Granick, *Langmuir*, 2006, **22**, 9495.
11 S. Jiang, M. J. Schultz, Q. Chen, J. S. Moore and S. Granick, *Langmuir*, 2008, **24**, 10073.
12 Z. Nie, W. Li, M. Seo, S. Xu and E. Kumacheva, *J. Am. Chem. Soc.*, 2006, **128**, 9408.
13 S. N. Yin, C. F. Wang, Z. Y. Yu, J. Wang, S. S. Liu and S. Chen, *Adv. Mater.*, 2011, **23**, 2915.
14 P. Garstecki, M. J. Fuerstman, H. A. Stone and G. M. Whitesides, *Lab Chip*, 2006, **6**, 437.
15 P. Garstecki, I. Gitlin, W. DiLuzio, G. M. Whitesides, E. Kumacheva and H. A. Stone, *Appl. Phys. Lett.*, 2004, **85**, 2649.
16 D. Dendukuri, D. C. Pregibon, J. Collins, T. A. Hatton and P. S. Doyle, *Nat. Mater.*, 2006, **5**, 365.
17 R. Erhardt, A. Böker, H. Zettl, H. Kaya, W. Pyckhout-Hintzen, G. Krausch, V. Abetz and A. H. E. Müller, *Macromolecules*, 2001, **34**, 1069.
18 R. Deng, S. Liu, F. Liang, K. Wang, J. Zhu and Z. Yang, *Macromolecules*, 2014, **47**, 3701.
19 A. H. Gröschel, A. Walther, T. I. Löbling, J. Schmelz, A. Hanisch, H. Schmalz and A. H. E. Müller, *J. Am. Chem. Soc.*, 2012, **134**, 13850.
20 S. Jiang and S. Granick, *Langmuir*, 2008, **24**, 2438.
21 D. Zerrouki, J. Baudry, D. Pine, P. Chaikin and J. Bibette, *Nature*, 2008, **455**, 380.
22 A. Walther, X. André, M. Drechsler, V. Abetz and A. H. E. Müller, *J. Am. Chem. Soc.*, 2007, **129**, 6187.
23 B. Liu, C. Zhang, J. Liu, X. Qu and Z. Yang, *Chem. Commun.*, 2009, 3871.
24 S. D. Kong, J. Lee, S. Ramachandran, B. P. Eliceiri, V. I. Shubayev, R. Lal and S. Jin, *J. Controlled Release*, 2012, **164**, 49.
25 L. O. Mair, B. Evans, A. R. Hall, J. Carpenter, A. Shields, K. Ford, M. Millard and R. Superfine, *J. Phys. D: Appl. Phys.*, 2011, **44**, 125001.
26 X. Feng, X. Guo and K. Qiu, *Makromol. Chem.*, 1988, **189**, 77.
27 L. Hu, Z. Chen and M. J. Serpe, *Soft Matter*, 2012, **8**, 1009.
28 Y. D. Liu, J. Lee, S. B. Choi and H. J. Choi, *Smart Mater. Struct.*, 2013, **22**, 065022.
29 B. J. Park, F. F. Fang and H. J. Choi, *Soft Matter*, 2010, **6**, 5246.
30 A. K. Vuppu, A. A. Garcia and M. A. Hayes, *Langmuir*, 2003, **19**, 8646.
31 H. Singh, P. E. Laibinis and T. A. Hatton, *Langmuir*, 2005, **21**, 11500.
32 N. T. Nguyen, G. Zhu, Y. C. Chua, V. N. Phan and S. H. Tan, *Langmuir*, 2010, **26**, 12553.
33 J. J. Benkoski, S. E. Bowles, B. D. Korth, R. L. Jones, J. F. Douglas, A. Karim and J. Pyun, *J. Am. Chem. Soc.*, 2007, **129**, 6291.
34 R. Rungsawang, J. Da Silva, C. P. Wu, E. Sivaniah, A. Ionescu, C. H. Barnes and N. J. Darton, *Phys. Rev. Lett.*, 2010, **104**, 255703.
35 J. Bacri and D. Salin, *J. Phys., Lett.*, 1982, **43**, 649.
36 F. Xu, C. M. Wu, V. Rengarajan, T. D. Finley, H. O. Keles, Y. Sung, B. Li, U. A. Gurkan and U. Demirci, *Adv. Mater.*, 2011, **23**, 4254.

Electronic Supplementary Material (ESI) for Soft Matter.

Supporting Information

Magnetic Field Assisted Programming of Particle Shapes and Patterns

*Wenwen Xu, Yuyu Yao, John S. Klassen, Michael J. Serpe**

Department of Chemistry, University of Alberta, Edmonton, Alberta, T6G 2G2, Canada

*Corresponding author email: michael.serpe@ualberta.ca

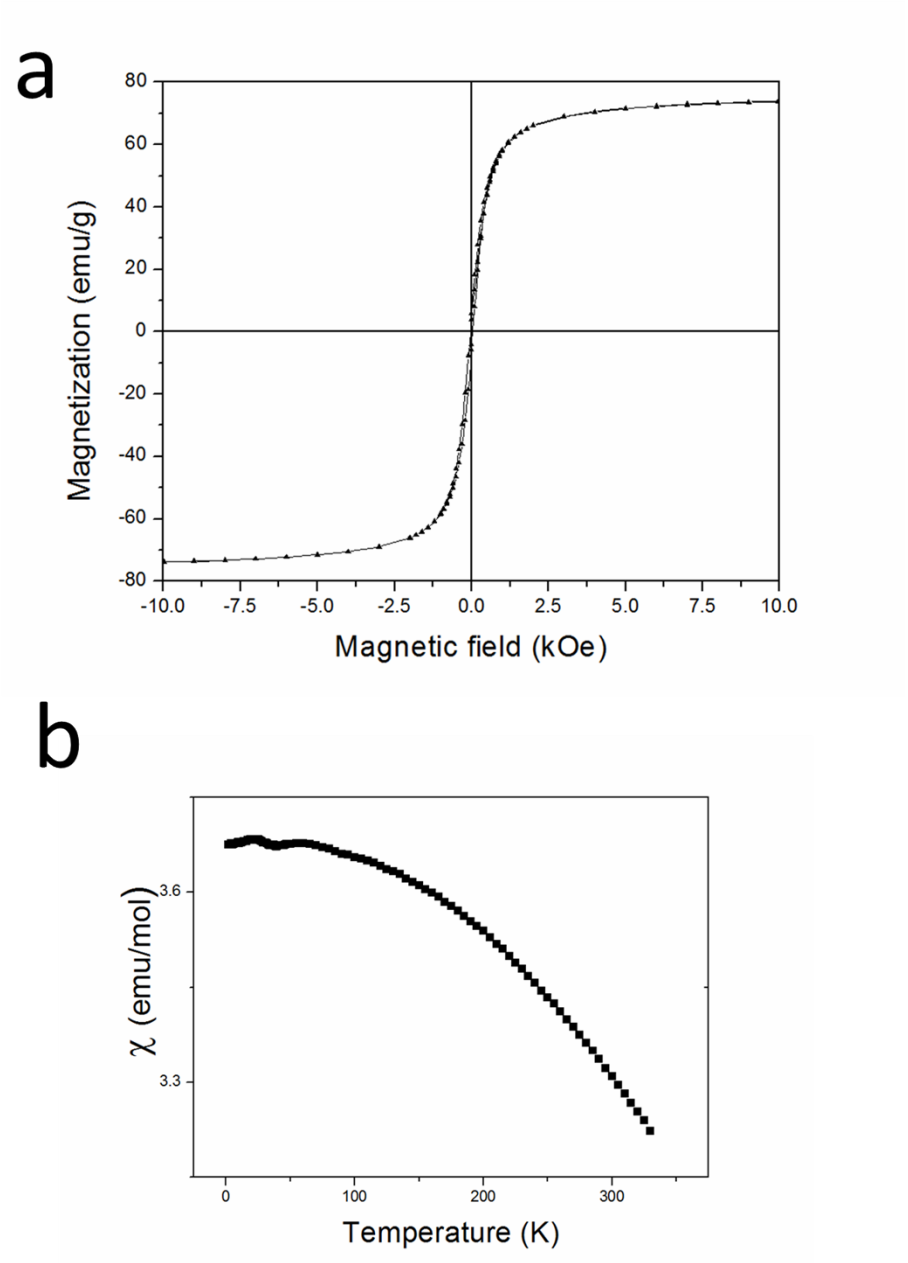

Figure S1. a) Magnetic hysteresis curves measured at room temperature for the MNPs. b) susceptibility (X) in different temperature.

The plots above show the MNPs purchased from Sigma are ferromagnetic. Accordingly, all the observations and explanations in the main text follow ferromagnetism theory.

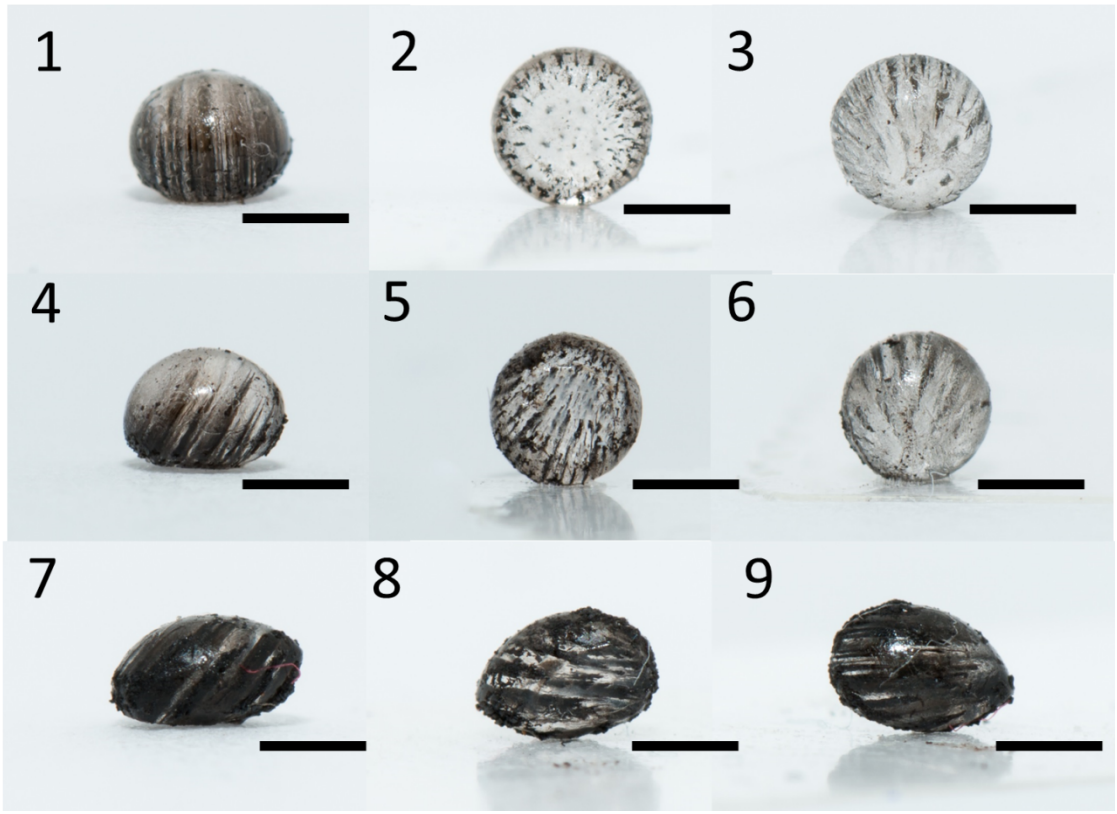

Figure S2. Photographs of the resulting particles polymerized with the magnet below the droplet at a distance of (1-3) 0.3 cm position (5,5) on the Teflon, (4-6) at a distance of 0.3 cm position (1,2) on the Teflon, and (7-9) at a distance of 0.3 cm position (1,2) on the Teflon, with the concentration of MNPs increased to 0.55 M. As can be seen, the shape of the particle depended on position, and the MNP concentration. All photographs on the left are side views, middle are bottom views, and right are top views. All scale bars in the pictures are 1mm.

Figure S3. Photographs of the resulting particles polymerized with the magnet above the droplet at a distance of (1-3) 5 cm, and (4-6) 4.5 cm. (7-9) First the magnet was <4.5 cm to make the rod structure as shown in (4-6), then moved to a distance of 5 cm. AS can be seen, the gravitational force pulls the rod back into the particle. (10-12) This is the same as (7-9), but the final distance of the magnet is 6 cm, which allows even more of the rod to enter the particle to make a stripe. All particles were synthesized at the (5,5) position. All photographs on the left are side views, middle are bottom views, and right are top views. All scale bars in the pictures are 1mm.

Figure S4. Photographs of the resulting particles polymerized with a magnet above and below the droplet in the attractive regime. (1-3) The distance between the top magnet and Petri dish is 5 cm and the distance between the bottom magnet and the Petri dish is 2 cm at position (5,5) on the Teflon. (4-6) The distance between the top magnet and Petri dish is 3.5 cm and the distance between the bottom magnet and Petri dish is 2 cm position (5,5) on the Teflon. All photographs on the left are side views, middle are bottom views, and right are top views. All scale bars in the pictures are 1mm.

Figure S5. Photographs of the resulting particles polymerized with a magnet above and below the droplet in the repulsive regime. For the photographs in (4-9, 16-18, 22-24) the left panel is a side view of the major axis, the middle panel is side view of the minor axis, and the right panel is a bottom view. Otherwise, all photographs on the left are side views, middle are bottom views, and right are top views. (1-3) The distance between the top magnet and Petri dish is 5 cm, and the distance between bottom magnet and the Petri dish is 2 cm, position (1,1) on the Teflon. (4-6) The distance between top magnet and Petri

dish is 4 cm, and the distance between bottom magnet and Petri dish is 2 cm, position (1,1) on the Teflon. (7-9) The distance between the top magnet and Petri dish is 3.5 cm, and the distance between bottom magnet and Petri dish is 2 cm, position (1,1) on the Teflon. (10-12) The distance between top magnet and Petri dish is 3 cm, and the distance between the bottom magnet and Petri dish is 2 cm, position (1,1) on the Teflon. (13-15) When the top magnet is closer than 3 cm to the Petri dish, and the distance between the bottom magnet and Petri dish is 2 cm the whole droplet floats to the surface of the TMP. (16-18) The distance between the top magnet and the Petri dish is 3 cm, and the distance between the bottom magnet and Petri dish is 1 cm, position (1,1) on the Teflon. (19-21) The distance between the top magnet and Petri dish is 5 cm, and the distance between bottom magnet and Petri dish is 0.3 cm, position (2,3) on the Teflon. (22-24) The distance between the top magnet and the Petri dish is 2.4 cm, and the distance between the bottom magnet and Petri dish is 0.3 cm, position (2,3) on the Teflon. All scale bars in the pictures are 1mm.

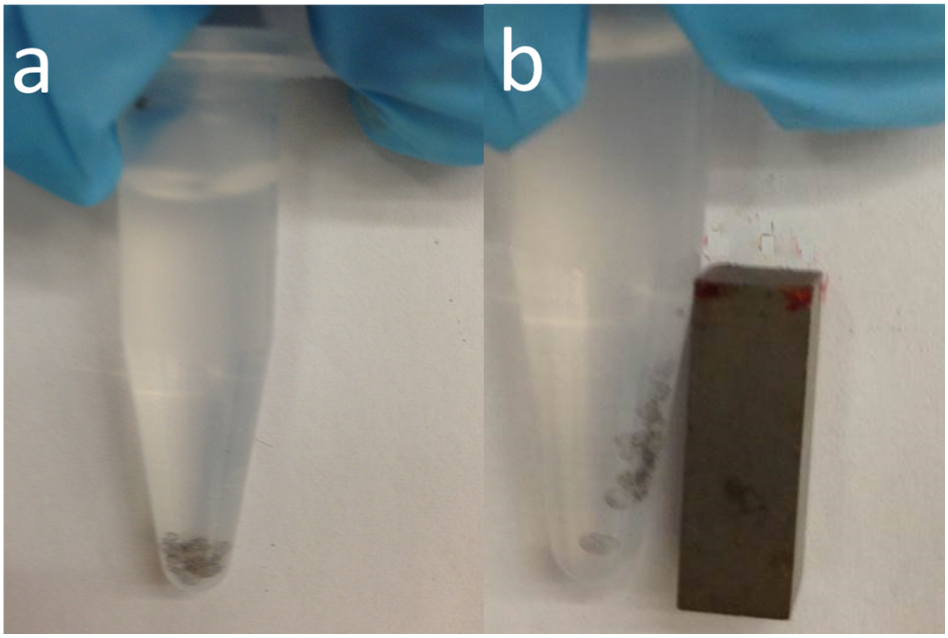

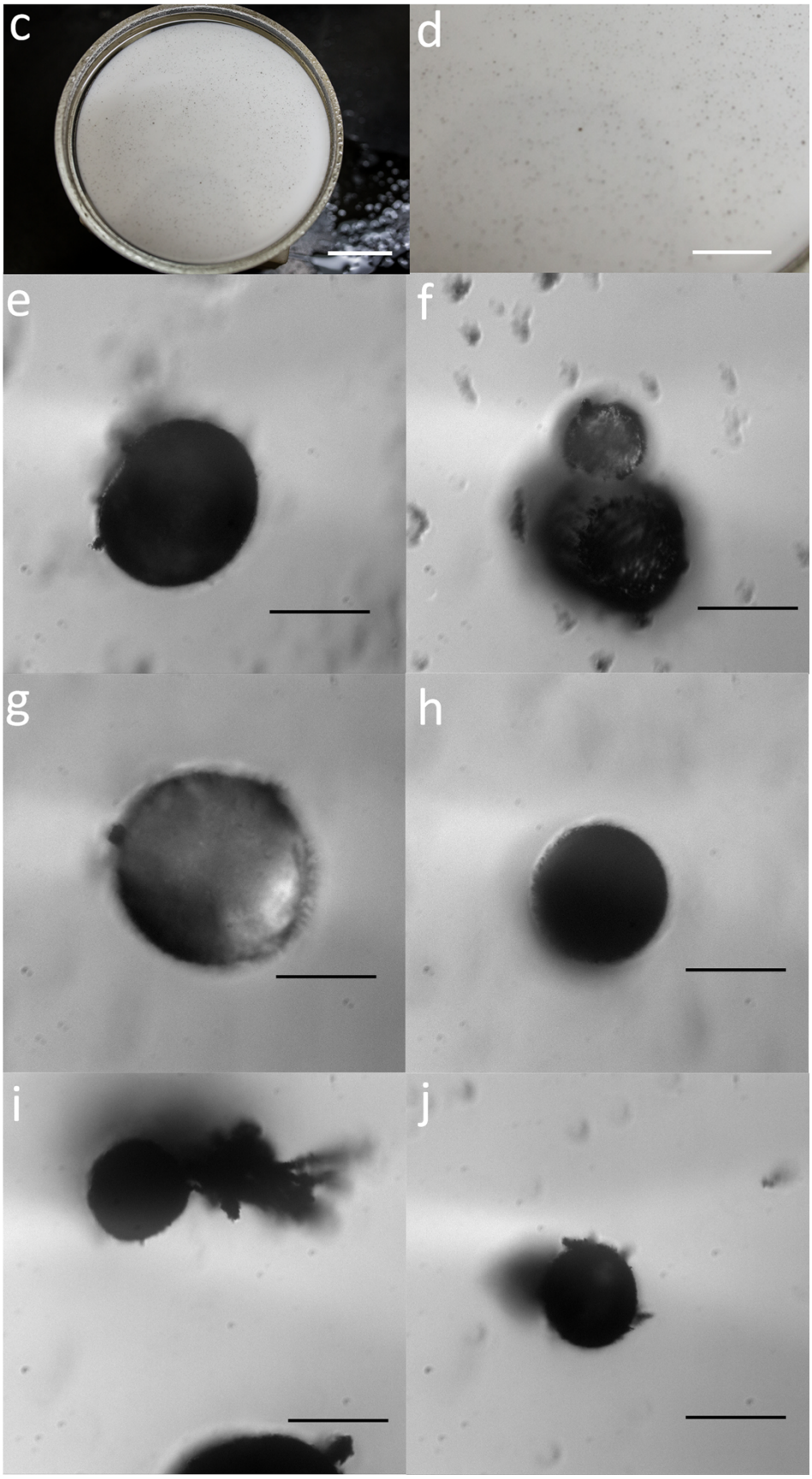
c
d
e
f
g
h
i
j

Figure S6. (a) Photograph of particles collected using the method in Figure 7(a); (b) their response to an external magnetic field; (c) droplets generated on Teflon using the method in Figure 7(b), which can be subsequently polymerized upon exposure to UV light, the scale bar is 2 cm; (d) zoom in of the Teflon film in (c), each black "dot" is an individual droplet that can be polymerized, scale bar is 1 cm; (e-j) photographs of *representative* particles generated from (c,d), scale bar is 50 μm.

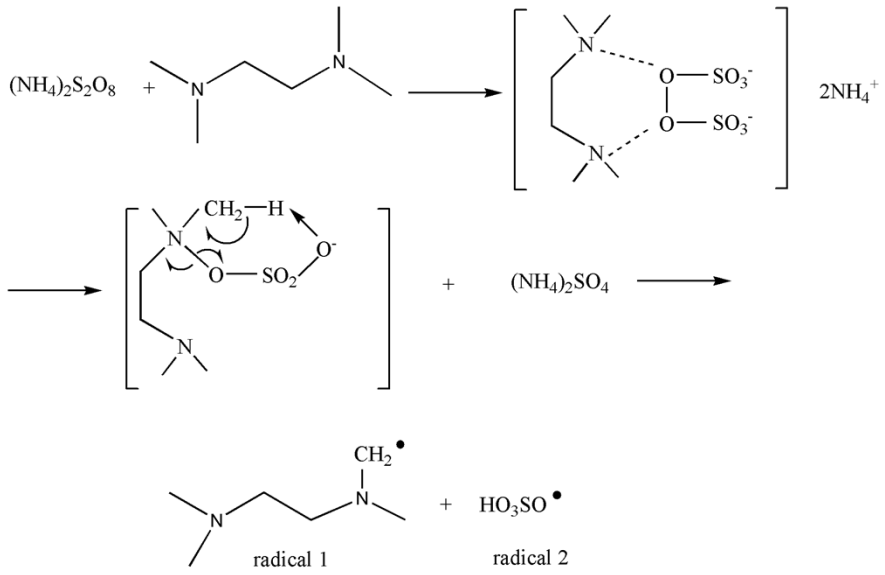

Figure S7. APS-TEMED reaction mechanism that is responsible for generating free radicals, which can subsequently initiate polymerization.

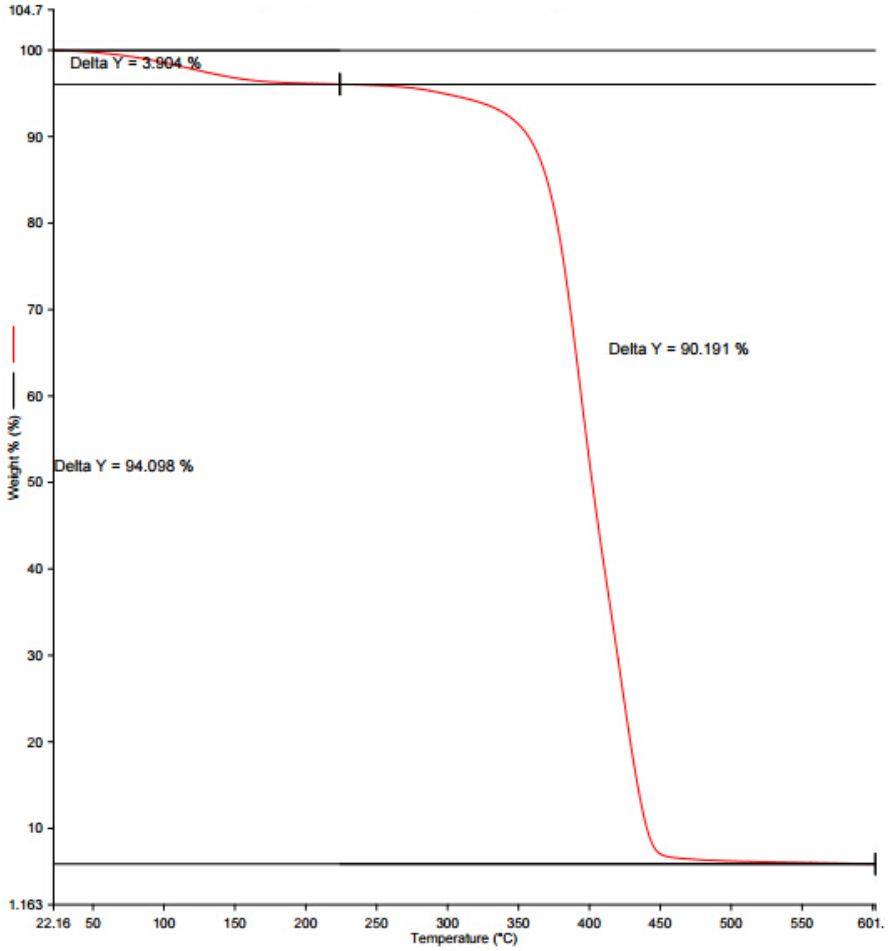

Figure S8. TGA results of the synthesized particles. The intial weight loss ~4% ("delta Y" at low temperature) is mainly due to the loss of residue water inside the polymer network. An additional ~90% is lost at high T ("delta Y" at high temperature) from the loss of polymer. From the data, we can determine that the mass of the MNPs is ~6% of the particle's total mass.